

A Cheap Polypyrrole-Derived Fe-N-C Electrocatalyst with Ultrahigh Oxygen Reduction Activity in Alkaline Electrolyte

Yao Liu^{1†}, Xiaojing Liu^{2†}, Junli Liu^{1†}, Chaozhong Guo^{1,*}, Yanrong Li³, Jin Zhang³, Zhongbin Li^{1,*}

¹ Research Institute for New Materials Technology, School of Materials and Chemical Engineering, Engineering Research Center of New Energy Storage Devices and Applications, Chongqing University of Arts and Sciences, Chongqing 402160, China.

² Ningbo Key Laboratory of Specialty Polymers, Faculty of Materials Science and Chemical Engineering, Ningbo University, Ningbo 315211, China

³ College of Materials Science and Engineering, Chongqing University of Technology, Chongqing 400054, China

†These authors equally contributed to this work, and they are considered as the co-first author.

*E-mail: guochaozhong1987@163.com (C. Guo); las1166@hotmail.com (Z. Li)

Received: 2 October 2018 / Accepted: 1 April 2019 / Published: 10 May 2019

Ternary Fe-N-C catalysts are regarded as the most promising candidates for low-cost alternatives to the Pt-based materials for catalyzing the oxygen reduction reaction (ORR). In this paper, the Fe and N codoped carbon catalyst (Fe-Py@K-800) with the unique foam-like 3D structure has been fabricated by using the molecular sieve as a new solid-state template. The results of physical characterization indicate that Fe atoms are coordinated with nitrogen atoms to form the Fe-N ORR-active structure. In contrast with the commercial Pt/C catalyst, the Fe-Py@K-800 displays a comparable ORR electrocatalytic activity with an onset potential of ~1.1 V and a half-wave potential of ~0.88 V (vs. RHE), however, the long-term stability of Fe-Py@K-800 is obviously better. These results show that iron-organic coordination in the pyrrole ring will play a role in the generation of nitrogen-rich active sites, which facilitates the enhancement of ORR activity in alkaline electrolyte.

Keywords: Porous carbon, Oxygen reduction, Electrocatalyst, Molecular sieve

1. INTRODUCTION

Oxygen reduction reaction (ORR) at the cathode is undoubtedly the pivot among various fuel cells and metal-air batteries, but as a kinetically slow process, which is a major limiting factor of energy-conversion efficiency in these technologies. Although Platinum (Pt)- and its alloys- based materials are the most frequently investigated catalysts for ORR due to their superior activity, the high cost and low abundance of the precious metals hinder their large-scale commercial applications[1, 2]. Consequently,

a series of alternative non-precious metal catalysts (NPMCs) have been developed to facilitate the ORR on electrodes, including metal free nitrogen-doped carbon [3-5], non-precious metal oxides and carbides [6,7], transition-metal-coordinating macrocyclic compounds [8, 9], and transition-metal-coordinating nitrogen-doped carbon catalysts.

Among various alternative NPMCs, the materials transition-metal-coordinating nitrogen-doped carbon catalysts (M-N/C) have been generally considered to be the most promising substitutes for PMG catalysts. The M-N/C catalysts as NPMCs have emerged and initiated tremendous research interest as potential alternative catalysts for ORR since they were discovered the ORR activity of cobalt phthalocyanine by Jasinski in 1964 [10]. Researchers have put much more effort and made great progresses in delicate selection of suitable transition metal, nitrogen and carbon precursors and optimization of the fabrication [11-18]. For example, Yeager proposed a model that electronically conducting surfaces with nitrogen groups was capable of binding transition metal species to form $M-N_x$ structure [11].

However, the long-term instability of transition metal macrocycles and the toxicity of metal dioxides are still highly desired because these properties are the primary function for ORR. Polypyrrole (PPY) materials show great potential for application in the preparation of electronic conductors and catalysts in batteries, electronic devices and electrochromic devices [19-22], owing to their reasonable thermal stability and high conductivity at room temperature. PPY is a chemical compound formed from a number of connected pyrrole ring structure which can be served as decent source for nitrogen and carbon in catalyst. Furthermore, the porous structure and high surface area of PPY could be employed as matrix to incorporate metallic catalysts for the reduction of oxygen [23,24]. These chemical features enhance their applicability for homogeneous distribution of metal nanoparticles and doping of heteroatoms simultaneously. In early research, PPY was mainly used as a substrate in the catalysts for ORR. For instance, Yuasa et al. [25] modified carbon particles with polypyrrole to adsorb on the cobalt ions as electrocatalytic site for oxygen reduction and found that the Co-modified PPY exhibited high catalysis towards ORR and displayed electrocatalytic activity for the four-electron reduction of O_2 . Qin et al. [26] developed a cobalt polypyrrole carbon (Co-PPY-C) composite, and probed metallo-organic coordination compounds towards ORR, in which PPY acted as a substrater other than a catalyst. Lee et al. [27] developed a carbon-supported cobalt polypyrrole (Co-PPy/C) electrocatalysts, and pointed out that the cobalt–nitrogen coordination could be the active sites towards ORR.

Herein, we have fabricated a novel kind of nanostructured non-precious metal ORR catalyst (Fe-Py@K-800) via one-step carbonization under nitrogen atmosphere, which does not require further to be activated. Iron modified on polypyrrole to form Fe-N bonding in pyrrole ring as active sites. Polypyrrole not only served as decent source for nitrogen and carbon in catalyst, but also enhanced its reasonable thermal stability and high conductivity. Cyclic voltammograms (CVs) and rotating ring-disk electrode (RRDE) revealed the kinetics of electrochemical catalytic ORR at the Fe-Py@K-800 was dominantly the four-electron reaction pathway. The SEM images, TEM and XPS spectra obviously indicated that this catalyst containing foam-like 3D nanostructure and Fe-N bonding. These facts should help in determining the structure of the active sites and in identifying methods to develop a novel approach for design of oxygen reduction catalyst.

2. EXPERIMENTAL

In a typical preparation, 0.2 g molecular sieve (KIT-6), 0.2 g ferric chloride and 20 mL of ethanol were mixed under stirring to form Fe-N with Fe-C at room temperature for 2h.. The mixture was tread by 0.2 g of pyrrole was added into with stirring for 30 min, and then 1.0 g of ammonium peroxydisulfate (APS) as an oxidizing agent was subsequently introduced and controlled the condition to PH= 2 by 0.5 M hydrochloric acid (HCl) solution. The polymerization was performed with vigorous stirring for 24 h at 25°C to promote the formation of polypyrrole on molecular sieve (KIT-6) surface. Then, the mixture was directly dehydrated under a vacuum at 100°C for 12 h to produce a Fe-modified polypyrrole precursor. At last, the precursor was heat-treated at different temperatures (700, 800, 900, and 950°C) for 2 h under N₂ protection to obtain a series of carbon-based catalysts (Fe-Py@K-700, Fe-Py@K-800, Fe-Py@K-900, and Fe-Py@K-950). The heating rate was kept at 10 °C min⁻¹. As a control, we also prepared Fe-Py-800 and Py-800 catalysts at 800°C on the same conditions of polypyrrole synthesis and heat-treatment.

High-resolution scanning electron microscopy (SEM) was obtained on a Hitachi UHR S4800 (Japan). Transmission electron microscopy (TEM) tests were performed on a FEI Tecnai-G2 F30 instrument. X-ray photoelectron spectroscopy (XPS) was done on a Kratos XSAM800 spectrometer. Raman spectroscopy data was obtained using Horiba HR800 Raman system with laser excitation wavelength of 514.5 nm.

The CHI760E Bipotentiostatic purchased from Shanghai Chenhua Instruments Co.Ltd., China was used to the electrochemical tests with a conventional three-electrode device. A glass-carbon rotation ring-disk electrode (GC-RRDE, Φ=5 mm, Pine Instrument Co.) was used as working electrode (WE), a saturated calomel electrode (SCE) worked as reference electrode (RE) and a graphite rod (Φ = 0.5 cm) was done on auxiliary electrode (AE). The fabrication of WE refers to our previous reports [12]. Generally, 10 μl of 10 mg ml⁻¹ dispersion was pipetted onto the GC-RRDE surface and naturally dried in air. The mass loading of carbon-based catalysts and commercial Pt/C catalyst (20 wt.% Pt, Aladdin Industrial Co. Ltd.) was controlled to be ~600 μg cm⁻². In order to sufficiently induce complete peroxide decomposition produced during the test, the ring potential was set at 0.5 V (vs. SCE) as reported elsewhere. The HO₂% yield and electron transfer number (n) during the ORR were calculated using the following equations [28]:

$$\% HO_2^- = 100 \times \frac{2I_r / N}{I_d + (I_r / N)} \quad (1)$$

$$n = 4 \times \frac{I_d}{I_d + I_r / N} \quad (2)$$

where I_d is the Faradaic current at the disk, I_r is the Faradaic current at the ring, and N is the collection efficiency of ring electrode (0.38). n was calculated from the Koutecky-Levich equation [29]:

$$1/j_d = 1/j_k + 1/B\omega^{1/2} \quad (3)$$

$$B = 0.62nFC_0D_0^{2/3}V^{-1/6}\omega^{1/2} \quad (4)$$

where F is the Faraday constant, Co is the O₂ saturation concentration in the electrolyte, D_O is the O₂ diffusion coefficient in the electrolyte, v is the kinetic viscosity of the electrolyte, and ω is the electrode rotation speed, and 0.62 is a constant when the rotation rate is expressed in rpm.

3. RESULTS AND DISCUSSION

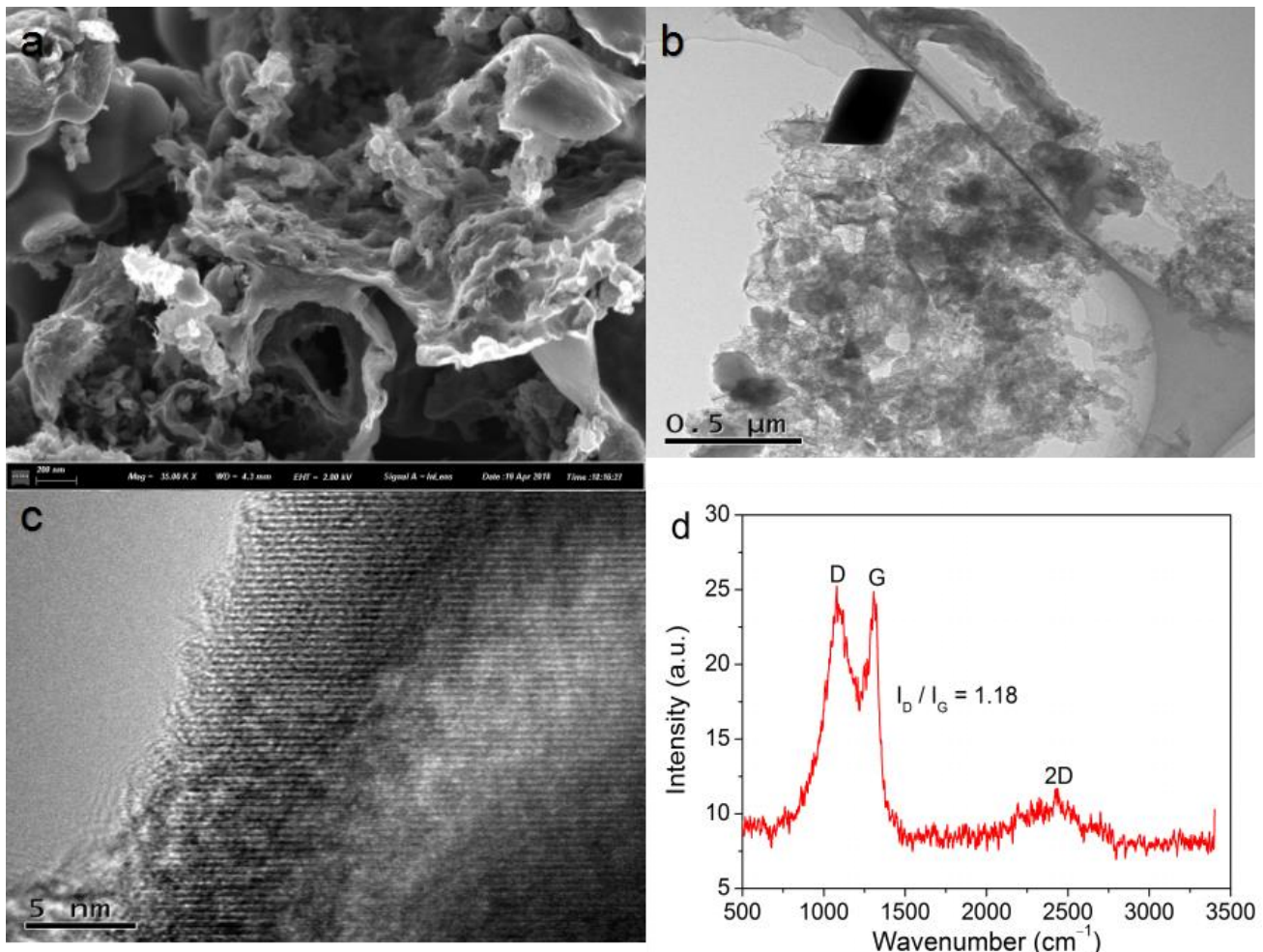


Figure 1. The SEM (a) and TEM (b,c) images of Fe-Py@K-800; The Raman spectrum of Fe-Py@K-800 (d).

Fig. 1 shows the SEM and TEM images of the Fe-Py@K-800 catalyst. The wave-like morphology can be observed obviously at the surface of the Fe-Py@K-800 catalyst and foam-like 3D porous nanostructure carbon has been formed inside. Besides, TEM images of Fe-Py@K-800 (Fig.1b) further support the results of SEM analysis. The formation of foam-like 3D porous nanostructure is substantially thanks to the role of the molecular sieve, with high mechanical strength which could be served as the template and skeleton to protect the carbonized resin structure from aggregation or collapse. To accommodate iron ions at a coordination site within the PPy layer, the PPy layer was produced at the surface of the molecular sieve with a high surface-area. When the molecular sieve has been hydrofluoric acid soaking, foam-like 3D porous nanostructure were obtained. Moreover, the Raman spectra of Fe-

Py@K-800 catalyst (Fig. 1d) exhibits two board bands, located at \sim 1345 and \sim 1590 cm⁻¹ for D band account for the disordered sp³ carbon (and G band attributed to graphitic sp² carbon, respectively[30]. The intensity ratio D band to G band (I_D/I_G) is a measurement of the disordered and graphitic degrees, in this case, the I_D/I_G ratios of Fe-Py@K-800 is about 1.18, indicating that iron-doping efficiency and more defected structure facilitate to increase the active site density and enhance the ORR electrocatalytic activity. The disordered and graphitic degrees further support the results of SEM (Fig1.c).

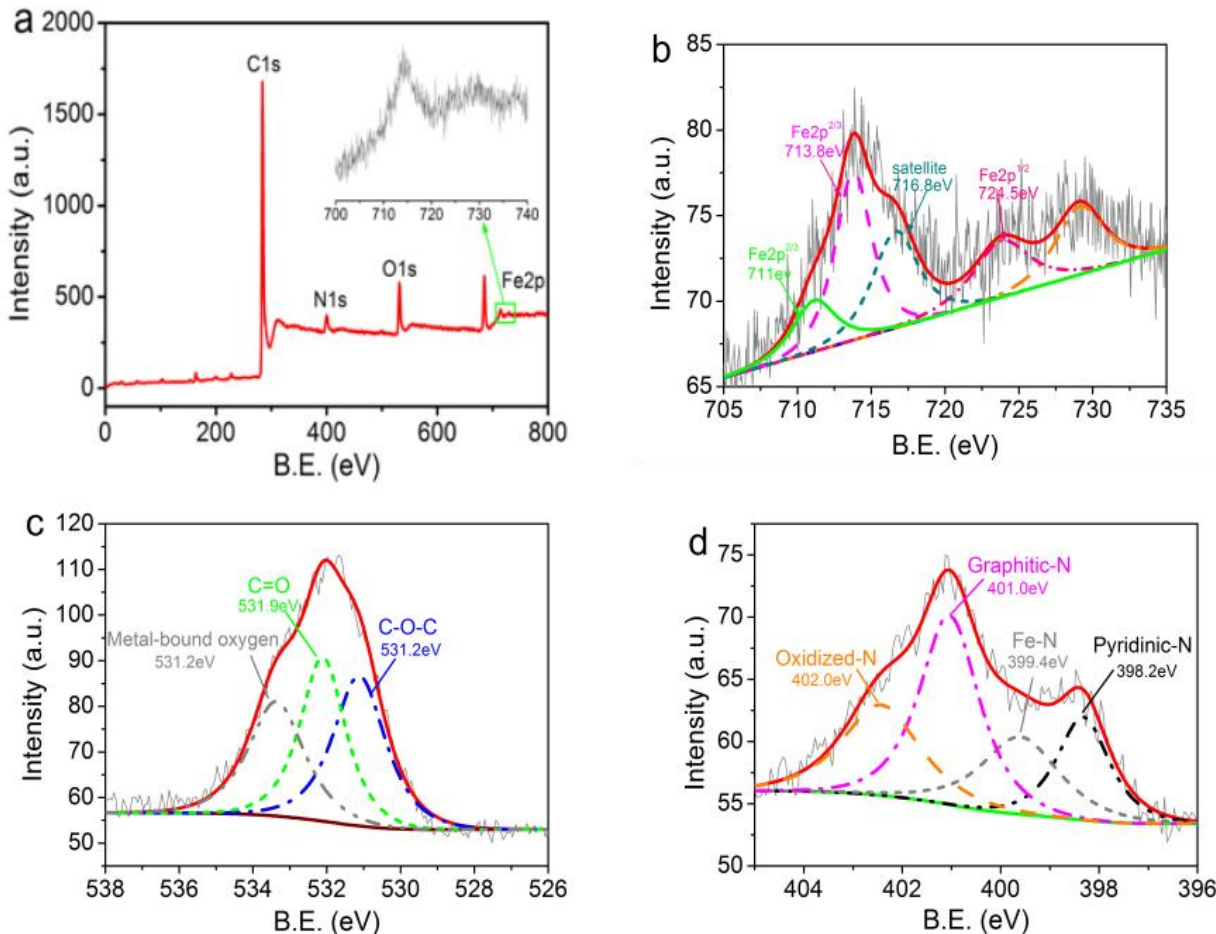


Figure 2. (a) XPS full-scan spectra of Fe-Py@K-800; XPS narrow-scan spectra for Fe 2p(a), O1s(b) and N 1s (d) regions of Fe-Py@K-800.

The XPS full survey spectrum of Fe-Py@K-800 is shown in Fig.2a. The chemical components of Fe-Py@K-800 are mainly nitrogen, carbon and oxygen. In addition, the XPS peak of metal Fe can be slightly found in catalyst. This indicates that the catalyst prepared from this method are doped with Fe and N. The surface Fe and N contents of Fe-Py@K-800 were 1.08 at.% and 5.0 at.%, respectively. Moreover, the high-resolution spectrum of Fe 2p XPS of Fe-Py@K-800 clearly shows three peaks at 708.4, 710.1, and 711.4 eV, respectively, which further verifies that the characteristic peak of the Fe 2p^{3/2}[31].The satellite peaks with B.E. of 717.1 eV at the high binding energy side of the main peaks with B.E. of 724.5eV were observed to be characteristic for Fe 2p^{1/2}[32]. Thus, The Fe plays a role in

connecting to the nitrogen in the pyrrole ring to form the metal-organic coordination compound in the catalyst.

The O 1s XPS spectrum of Fe-Py@K-800 (Fig. 2c) shows three peaks at 531.2, 531.9 and 533.0 eV, which can be attributed to C(aliphatic)-O-C(aliphatic), C=O, and metal-bounded oxygen (Fe-O) [33, 34], respectively. The N1s of Fe-Py@K-800 show peaks at 398.2, 399.4, 401.0, and 402.0 eV (Fig. 2d), corresponding to pyridinic-N, Fe-N compounds, graphitic-N, and oxidized nitrogen compounds [35-38], with compositions of 18.9, 20.2, 37.9, and 23.6 at.%, respectively. The reason for the improved catalytic activity of Fe-Py@K-800 can be related to the large number of N atoms in pyrrole ring, polypyrrole can facilitate the formation of N-C. The graphitic N content were 37.9 at.% in total doped nitrogen and high Fe-N content of compounds were 20.2 at.%, which further verifies that the presence of Fe-N bond existed in Fe2p spectrum. All of the above results indicate that Fe atoms are mainly in two forms including Fe-N and Fe-O in the Fe-Py@K-800.

We have measured the CV curves in N₂ versus O₂-saturated 0.1 M KOH solution of Fe-Py@K-800. The onset potential of Fe-Py@K-800 is found to be nearly 1.1 V vs. RHE in O₂-saturated electrolyte. For comparison, the electrocatalytic activities of the catalysts in N₂-saturated electrolyte, there is no visible peak (Fig. 3a). Above results qualitatively suggest an ORR electrocatalytic activity of Fe-Py@K-800. To gain insight into the active sites of Fe-Py@K-800, the effect of pyrolysis temperature were investigated by LSV measurements (Fig. 3b). The Fe-Py@K-800 exhibits the highest ORR performance and the half-wave potential is found to be ~0.88 V vs. RHE which is about 22 mV higher than that of a commercial Pt/C catalyst (0.86 V vs. RHE). Therefore, the results suggest that a reaction temperature of 800 °C is the most favorable and it leads to the performance of this novel catalyst being superior to that of noble metals. As illustrated in Fig. 3c, the pyrolysis temperature affects the ORR peak potential (E_p), onset potential (E_{ORR}), half-wave potential (E_{1/2}) and limited current density (J) at 0.3 V vs. RHE of the catalysts, the 800 °C is the most favorable and it leads to the best electrochemical parameters. Tafel polarization curves of the catalysts (Fe-Py@K-700, 800, 900 and Pt/C) were compared by E as a function of log (J) (Fig. 3d), Tafel slopes are 114 (Fe-Py@K-700), 106 (Fe-Py@K-800), 111 (Fe-Py@K-900), and 79 mV dec⁻¹ (Pt/C), respectively. Lower Tafel slope values correspond to a large decrease in over-potential with the current density, which facilitates the enhancement of the ORR electrocatalytic activity. It is significant that the similarity in the Tafel slope values between Fe-Py@K-800 and commercial Pt/C catalyst implies the same ORR catalysis mechanism: the protonation of O²⁻ on the active sites of catalyst is the main rate-determining step [39].

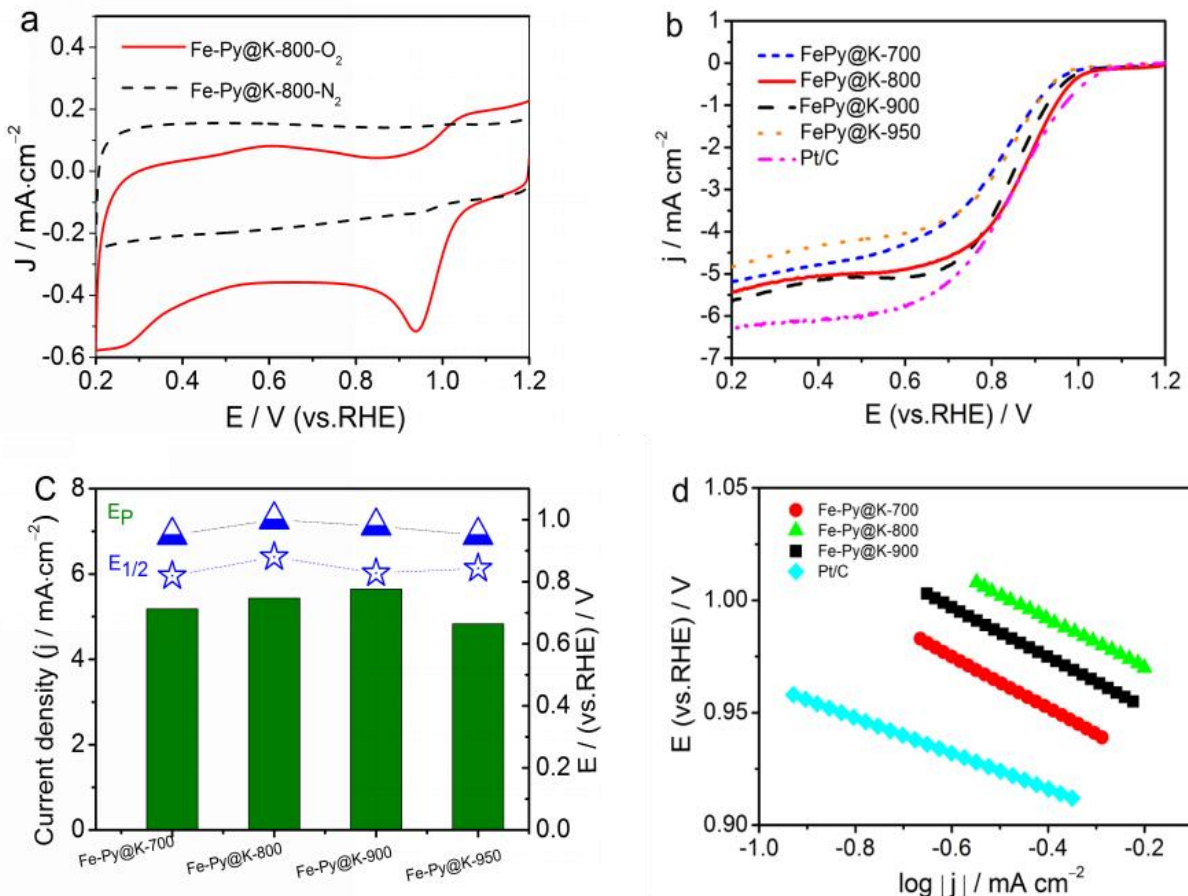


Figure 3. (a) CV curves of Fe-Py@K-800 in 0.1 M KOH solution saturated by O_2 , (b) LSV curves at the rotation rate of 1600 rpm for various catalysts, and (c) current density at 0.3 V (vs. RHE), onset-potential and the half-wave potential of different catalysts obtained from their LSV curves. (d) Tafel polarization plots of five GD-based catalysts to the ORR; the data obtained from (b). (A colour version of this figure can be viewed online.)

To explore the component impact on structure-catalytic activity and intrinsic electrocatalytic activity, Fig. 4a and 4b indicate the results of CV and LSV measurements for the activity of polypyrrole-based catalysts in 0.1 M KOH solution saturated by oxygen. PPY-Fe-800 catalyst has the highest ORR activity among the other two catalysts. The peak potential follows the trend of PPY-Fe-800 ($E_p = 0.88 \text{ V}$, $E_{1/2} = 0.82 \text{ V}$) > PPY-800 ($E_p = 0.82 \text{ V}$ and $E_{1/2} = 0.71 \text{ V}$). Additionally, the limited current density of PPY-Fe-800 at the potential of 0.5 V is nearly two times larger than that of PPY-800. The catalyzed electrode made with the Fe-Py@K-800 catalyst exhibits the best ORR activity with a onset potential of 1 V and a half-wave potential of 0.88 V in alkaline medium. We attribute the efficiency to the doping of Fe atoms in pyrrole ring, thus increasing the ORR catalytic activity. The high catalytic performance may be attributed to the molecular sieve developing the necessary porous structure and avoiding large weight loss and nitrogen evaporation during the process of direct pyrolysis, which leads to catalysts have a high density of active sites. The current density difference is due to the accessible active sites and mass transport property. Fig. 3c exhibits the LSV curves of Fe-Py@K-800 at rotation rates from 400 to 2500 rpm . The relationship between limiting diffusion current density and the rotation rate due is observed. This allows us to compute the number of exchanged electrons (n) for the ORR by the Koutecky–Levich

(K-L) plots drawn from the LSV curves at different rotating speeds (Fig. 4d). As calculated, the average electron transfer number of Fe-Py@K-800 during the reaction is 4.2 for a wide potential range from 0.2 V to 0.6 V (vs. RHE), suggesting a direct 4-electron transfer pathway toward oxygen reduction [40].

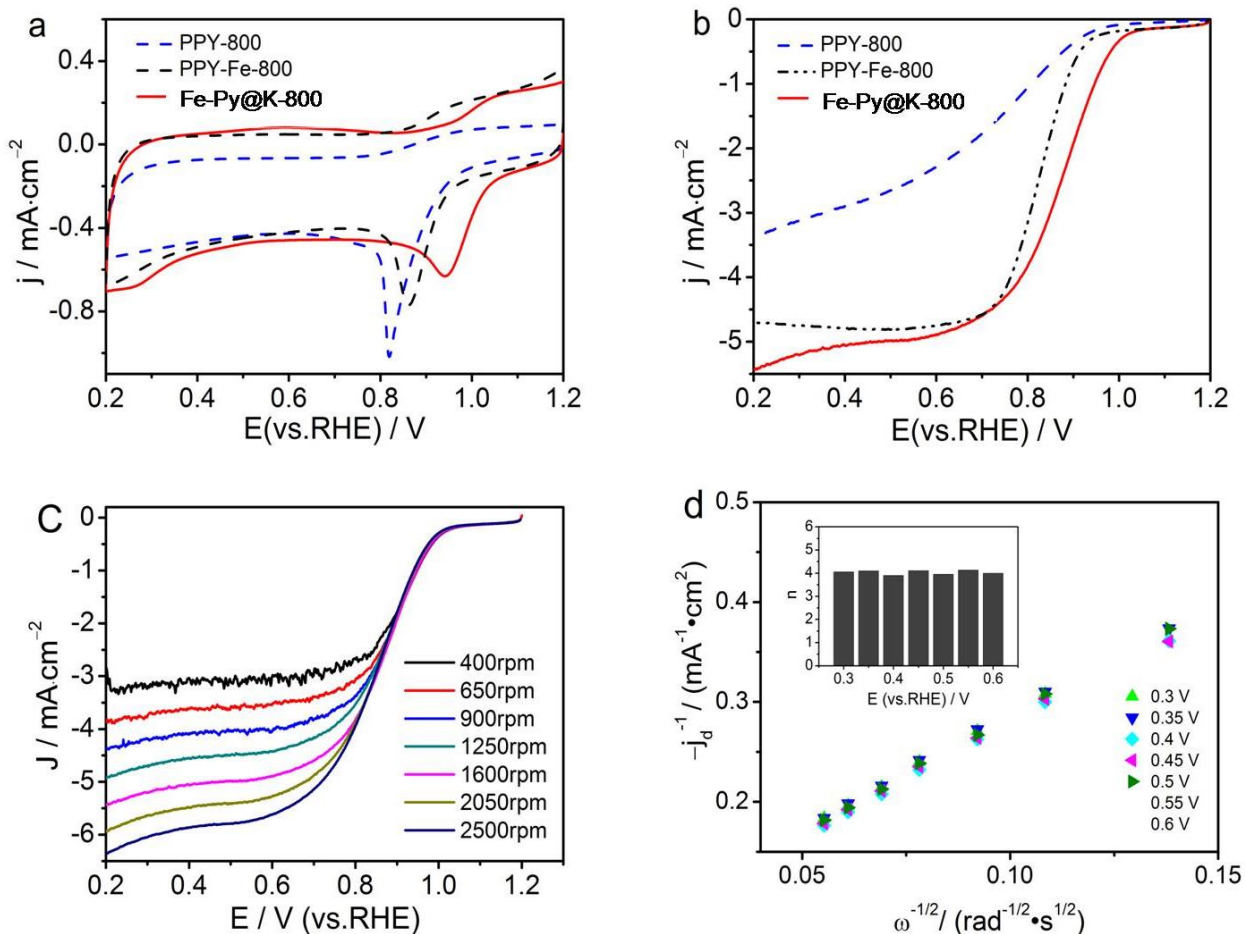


Figure 4. (a) CV and (b) LSV curves of PPy-800, PPy-Fe-800, Fe-Py@K-800 in O_2 -saturated 0.1 M KOH solution, (c) LSV curves of Fe-Py@K-800 in O_2 -saturated 0.1 M KOH solution at different rotation speeds (400-2500 rpm); (d) Koutecky-Levich plots of j_d^{-1} vs. $\omega^{-1/2}$ obtained from (c) at given potentials.

To better understand the ORR kinetics behavior of carbon-based catalysts in oxygen reduction, the yield of peroxide species and the electron transfer number were carefully examined by RRDE tests. As shown in Fig. 4a, the ring current (i_r) is much smaller than the disk current, and the current is only ~0.23 mA after the expansion of 20 times, but the H_2O_2 yield shows a typical increase with ring current (i_r). The measured H_2O_2 yield relative to the total reduction products for Fe-Py@K-800 is about 4% over the potential range from 0.2 to 0.6 V vs. RHE. A low yield of H_2O_2 is beneficial for the membrane electrode assemblies and maintaining the cell performance. This process which the yields correspond to an average electron transfer number of 3.9 follows a four-electron reaction pathway and is similar to the Pt/C catalyst. We attribute the Fe-doping causes a remarkable synergistic effect, thus increasing the electrochemical activity for the ORR., which suggests that it is one of the best non-noble metal

electrocatalysts for the ORR among all the other catalysts. The stability of Fe-Py@K-800 was also assessed in O₂-saturated 0.1 M KOH electrolyte by cycling the catalyst between 0.2 V and 1.2 V vs. RHE at 200 mV s⁻¹. After 2000 continuous cycles, the Fe-Py@K-800 modified electrode showed a 0.5 mA cm⁻² decline in the limiting current density, but no negative shift in onset potential and half-wave potential was observed (Fig. 5c), however, the onset potential and half-wave potential on Pt/C has decreased about 20 mV. The results prove that Fe-Py@K-800 exhibits durable operational stability, which is obviously superior to the Pt/C catalyst. The obtained electrochemical parameters regarding half-wave potential ($E_{1/2}$) and limited current density (J) at 0.3 V vs. RHE before and after AAT test are indicated in Fig. 5c.

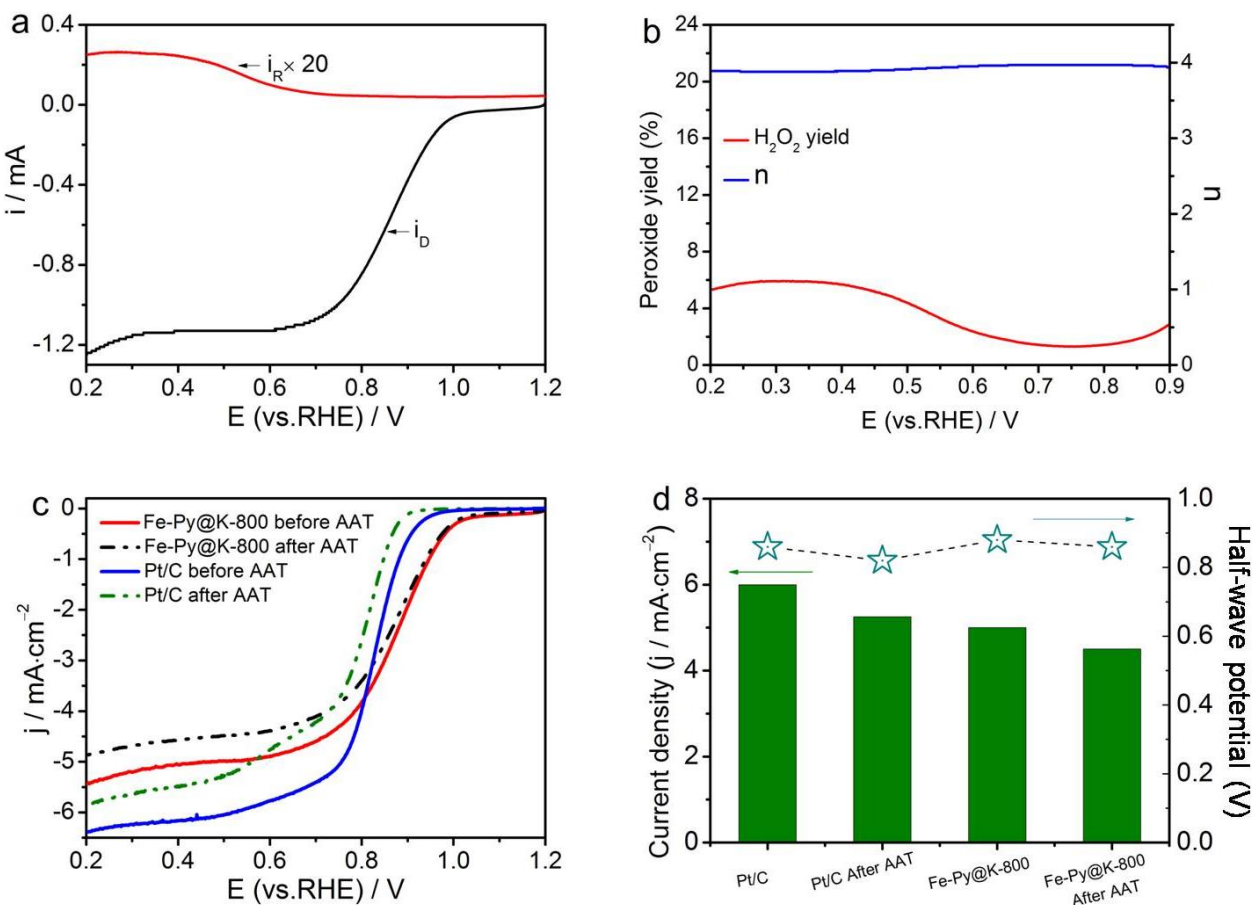


Figure 5. (a) Disk and ring currents obtained with LSV on RRDE for Fe-Py@K-800 in O₂-saturated 0.1 M KOH solution; (b) The corresponding electron transfer number and H₂O₂ yield from (a); (c) LSV curves of Fe-Py@K-800 and Pt/C in O₂-saturated 0.1 M KOH electrolytes before and after AAT tests. (d) Current density at 0.3 V (vs. RHE) and the half-wave potential of Pt/C and Fe-Py@K-800 catalyst obtained from (c).

4. CONCLUSIONS

In summary, we have demonstrated a route to the facile and cost-effective fabrication of the unique Fe-Py@K-800 nanostructures by a straightforward pyrolysis. Compared with the Pt/C, the Fe-Py@K-800 nanostructures can immensely reduce the costs while developing non-precious metals for

use as electrode catalysts. In this catalyst system, the Fe-N structure as an electron donor for ORR to generate active sites , which is attributed to that Fe atom is linked to nitrogen atom in the pyrrole ring , increasing the catalytic properties. The CV results revealed that the Fe-Py@K-800 exhibits superior in the catalytic activity and the kinetics of ORR beyond the Pt/C, those properties are beneficial for advance the coulomb efficiency of FCs. As a result, the Fe-Py@K-800 with cost-effective and superior electrochemical performance will open up a new involving the ORR. Finally, the Fe-Py@K-800 catalyst in alkaline electrolyte indicates its promising application for alternative cathode material for various fuel cells.

ACKNOWLEDGEMENTS

This study was financially supported by the National Natural Science Fund of China (No: 21805024), the Basic and Frontier Research Program of Chongqing Municipality (cstc2018jcyjAX0461), the Open Project of Engineering Research Center of New Energy Storage Devices and Applications of Chongqing Municipality (KF20170201), the Scientific and Technological Research Program of Chongqing Municipal Education Commission (KJ1711289) and the Student Scientific Research Program of Chongqing University of Arts and Sciences (M2017ME1).

References

1. M.K. Debe, *Nature*, 486 (2012) 43.
2. J. Wu, H. Yang, *Accounts Chem. Res.*, 46 (2013) 1848.
3. T. Chen, Z. Cai, Z. Yang, L. Li, X. Sun, T. Huang, A. Yu, H.G. Kia, H. Peng, *Adv. Mater.*, 23 (2011) 4620.
4. D. Deng, X. Pan, L. Yu, Y. Cui, Y. Jiang, J. Qi, W.-X. Li, Q. Fu, X. Ma, Q. Xue, G. Sun, X. Bao, *Chem. Mater.*, 23 (2011) 1188.
5. Y. Zheng, Y. Jiao, J. Chen, J. Liu, J. Liang, A. Du, W. Zhang, Z. Zhu, S.C. Smith, M. Jaroniec, G.Q. Lu, S.Z. Qiao, *J. Am. Chem. Soc.*, 133 (2011) 20116.
6. H.-Y. Su, Y. Gorlin, I.C. Man, F. Calle-Vallejo, J.K. Nørskov, T.F. Jaramillo, J. Rossmeisl, *Phys. Chem. Chem. Phys.*, 14 (2012) 14010.
7. D.V. Esposito, J.G. Chen, *Energ. Environ. Sci.*, 4 (2011) 3900.
8. C.T. Carver, B.D. Matson, J.M. Mayer, *J. Am. Chem. Soc.*, 134 (2012) 5444.
9. S. Samanta, K. Sengupta, K. Mittra, S. Bandyopadhyay, A. Dey, *Chem. Commun (Camb)*, 48 (2012) 7631.
10. R. Jasinski, *Nature*, 201 (1964) 1212.
11. S. Gupta, D. Tryk, I. Bae, W. Aldred, E. Yeager, *J. Appl. Electrochem.*, 19 (1989) 19.
12. J. Liang, R.F. Zhou, X.M. Chen, Y.H. Tang, S.Z. Qiao, *Adv. mater.*, 26 (2014) 6074.
13. J. Tian, A. Morozan, M.T. Sougrati, M. Lefevre, R. Chenitz, J.P. Dodelet, D. Jones, F. Jaouen, *Angew. Chem. Int. Ed. Engl.*, 52 (2013) 6867.
14. L. Lin, Q. Zhu, A.W. Xu, *J. Am. Chem. Soc.*, 136 (2014) 11027.
15. Y. Zhao, K. Watanabe, K. Hashimoto, *J. Am. Chem. Soc.*, 134 (2012) 19528.
16. Z.S. Wu, L. Chen, J. Liu, K. Parvez, H. Liang, J. Shu, H. Sachdev, R. Graf, X. Feng, K. Mullen, *Adv. mater.*, 26 (2014) 1450.
17. Z. Wen, S. Ci, F. Zhang, X. Feng, S. Cui, S. Mao, S. Luo, Z. He, J. Chen, *Adv. mater.*, 24 (2012) 1399.
18. W.J. Jiang, L. Gu, L. Li, Y. Zhang, X. Zhang, L.J. Zhang, J.Q. Wang, J.S. Hu, Z. Wei, L.J. Wan, *J. Am. Chem. Soc.*, 138 (2016) 3570.

19. T. Gunji, R.H. Wakabayashi, S.H. Noh, B. Han, F. Matsumoto, F.J. DiSalvo, H.D. Abruña, *Electrochim. Acta*, 283 (2018) 1045.
20. Y. Huang, H. Li, Z. Wang, M. Zhu, Z. Pei, Q. Xue, Y. Huang, C. Zhi, *Nano Energy*, 22 (2016) 422.
21. Z. Lin, G.H. Waller, Y. Liu, M. Liu, C.P. Wong, *Nano Energy*, 2 (2013) 241.
22. G. Xu, B. Ding, P. Nie, L. Shen, J. Wang, X. Zhang, *Chem.*, 19 (2013) 12306.
23. B. Wang, *J. Power Sources*, 152 (2005) 1.
24. R. Bashyam, P. Zelenay, *Nature*, 443 (2006) 63.
25. Makoto Yuasa, , Aritomo Yamaguchi, Hisayuki Itsuki, Ken Tanaka, A. Masakuni Yamamoto, K. Oyaizu, *Chem. Mater.*, 17 (2005).
26. H.Y. Qin, Z.X. Liu, W.X. Yin, J.K. Zhu, Z.P. Li, *J. Power Sources*, 185 (2008) 909.
27. K.-Q. Ding, F.-M. Cheng, *Synthetic Met.*, 159 (2009) 2122.
28. Y. Li, W. Liao, Z. Li, T. Feng, L. Sun, C. Guo, J. Zhang, J. Li, *Carbon*, 125 (2017).
29. T. Kikuchi, *Russian J. Electrochem.*, 38 (2002) 1364.
30. J. Zhou, X. Gao, R. Liu, Z. Xie, J. Yang, S. Zhang, G. Zhang, H. Liu, Y. Li, J. Zhang, Z. Liu, *J. Am. Chem. Soc.*, 137 (2015) 7596.
31. T. Yamashita, P. Hayes, *Appl. Surf. Sci.*, 254 (2008) 2441.
32. K. Ihm, T.-H. Kang, D.H. Lee, S.-Y. Park, K.-J. Kim, B. Kim, J.H. Yang, C.Y. Park, *Surf. Sci.*, 600 (2006) 3729.
33. H. Estrade-Szwarckopf, *Carbon*, 42 (2004) 1713.
34. L. Qiao, Y. Duan, Q. Zhao, F. Pan, B. Zhang, J. Zhang, *J. Surf. Coll.*, 30 (2014) 8238.
35. C. Guo, B. Wen, W. Liao, Z. Li, L. Sun, C. Wang, Y. Wu, J. Chen, Y. Nie, J. Liao, C. Chen, *J. Alloy. Compd.*, 686 (2016) 874.
36. W. Ding, Z. Wei, S. Chen, X. Qi, T. Yang, J. Hu, D. Wang, L.J. Wan, S.F. Alvi, L. Li, *Angew. Chem.*, 52 (2013) 11755.
37. Y. Nie, X. Xie, S. Chen, W. Ding, X. Qi, Y. Wang, J. Wang, W. Li, Z. Wei, M. Shao, *Electrochim. Acta*, 187 (2016) 153.
38. C. Guo, W. Liao, Z. Li, C. Chen, *Carbon*, 85 (2015) 279.
39. Z. Wu, J. Wang, L. Han, R. Lin, H. Liu, H.L. Xin, D. Wang, *Nanoscale*, 8 (2016) 4681.
40. X. Fu, Y. Liu, X. Cao, J. Jin, Q. Liu, J. Zhang, *Appl. Catal. B-Environ.*, 130-131 (2013) 143.